

## RADIO DETECTION OF LAT PSRs J1741–2054 AND J2032+4127: NO LONGER JUST GAMMA-RAY PULSARS

F. CAMILO<sup>1</sup>, P. S. RAY<sup>2</sup>, S. M. RANSOM<sup>3</sup>, M. BURGAY<sup>4</sup>, T. J. JOHNSON<sup>5,6</sup>, M. KERR<sup>7</sup>, E. V. GOTTHELF<sup>1</sup>, J. P. HALPERN<sup>1</sup>, J. REYNOLDS<sup>8,9</sup>, R. W. ROMANI<sup>10</sup>, P. DEMOREST<sup>3</sup>, S. JOHNSTON<sup>8</sup>, W. VAN STRATEN<sup>11</sup>, P. M. SAZ PARKINSON<sup>12</sup>, M. ZIEGLER<sup>12</sup>, M. DORMODY<sup>12</sup>, D. J. THOMPSON<sup>5</sup>, D. A. SMITH<sup>13,14</sup>, A. K. HARDING<sup>5</sup>, A. A. ABDO<sup>2,20</sup>, F. CRAWFORD<sup>15</sup>, P. C. C. FREIRE<sup>16</sup>, M. KEITH<sup>8</sup>, M. KRAMER<sup>17,18</sup>, M. S. E. ROBERTS<sup>19</sup>, P. WELTEVREDE<sup>8</sup>, AND K. S. WOOD<sup>2</sup>

<sup>1</sup> Columbia Astrophysics Laboratory, Columbia University, New York, NY 10027, USA

<sup>2</sup> Space Science Division, Naval Research Laboratory, Washington, DC 20375, USA

<sup>3</sup> National Radio Astronomy Observatory, Charlottesville, VA 22903, USA

<sup>4</sup> INAF—Osservatorio Astronomico di Cagliari, 09012 Capoterra, Italy

<sup>5</sup> NASA Goddard Space Flight Center, Greenbelt, MD 20771, USA

<sup>6</sup> University of Maryland, College Park, MD 20742, USA

<sup>7</sup> Department of Physics, University of Washington, Seattle, WA 98195, USA

<sup>8</sup> Australia Telescope National Facility, CSIRO, Epping, NSW 1710, Australia

<sup>9</sup> CSIRO Parkes Observatory, Officer-in-Charge for life, Parkes, NSW 2870, Australia

<sup>10</sup> Department of Physics, Stanford University, Stanford, CA 94305, USA

<sup>11</sup> Centre for Astrophysics and Supercomputing, Swinburne University of Technology, Hawthorn, Vic 3122, Australia

<sup>12</sup> Santa Cruz Institute for Particle Physics, Department of Physics and Department of Astronomy and Astrophysics, University of California at Santa Cruz, CA 95064, USA

<sup>13</sup> CNRS/IN2P3, Centre d'Études Nucléaires de Bordeaux-Gradignan, Gradignan, 33175, France

<sup>14</sup> Université de Bordeaux, Centre d'Études Nucléaires de Bordeaux-Gradignan, Gradignan, 33175, France

<sup>15</sup> Department of Physics and Astronomy, Franklin and Marshall College, Lancaster, PA 17604, USA

<sup>16</sup> NAIC, Arecibo Observatory, Arecibo, PR 00612, USA

<sup>17</sup> MPIfR, 53121 Bonn, Germany

<sup>18</sup> Jodrell Bank Centre for Astrophysics, University of Manchester, Manchester M13 9PL, UK

<sup>19</sup> Eureka Scientific, Inc., Oakland, CA 94602, USA

Received 2009 June 3; accepted 2009 August 20; published 2009 October 7

### ABSTRACT

Sixteen pulsars have been discovered so far in blind searches of photons collected with the Large Area Telescope on the *Fermi Gamma-ray Space Telescope*. We here report the discovery of radio pulsations from two of them. PSR J1741–2054, with period  $P = 413$  ms, was detected in archival Parkes telescope data and subsequently has been detected at the Green Bank Telescope (GBT). Its received flux varies greatly due to interstellar scintillation and it has a very small dispersion measure of  $DM = 4.7$  pc cm<sup>-3</sup>, implying a distance of  $\approx 0.4$  kpc and possibly the smallest luminosity of any known radio pulsar. At this distance, for isotropic emission, its gamma-ray luminosity above 0.1 GeV corresponds to 28% of the spin-down luminosity of  $\dot{E} = 9.4 \times 10^{33}$  erg s<sup>-1</sup>. The gamma-ray profile occupies 1/3 of pulse phase and has three closely spaced peaks with the first peak lagging the radio pulse by  $\delta = 0.29 P$ . We have also identified a soft *Swift* source that is the likely X-ray counterpart. In many respects PSR J1741–2054 resembles the Geminga pulsar. The second source, PSR J2032+4127, was detected at the GBT. It has  $P = 143$  ms, and its  $DM = 115$  pc cm<sup>-3</sup> suggests a distance of  $\approx 3.6$  kpc, but we consider it likely that it is located within the Cyg OB2 stellar association at half that distance. The radio emission is nearly 100% linearly polarized, and the main radio peak precedes by  $\delta = 0.15 P$  the first of two narrow gamma-ray peaks that are separated by  $\Delta = 0.50 P$ . The second peak has a harder spectrum than the first one, following a trend observed in young gamma-ray pulsars. Faint, diffuse X-ray emission in a *Chandra* image is possibly its pulsar wind nebula. The wind of PSR J2032+4127 is responsible for the formerly unidentified HEGRA source TeV J2032+4130. PSR J2032+4127 is coincident in projection with MT91 213, a Be star in Cyg OB2, although apparently not a binary companion of it.

**Key words:** gamma rays: observations – ISM: individual (TeV J2032+4130) – open clusters and associations: individual (Cyg OB2) – pulsars: individual (PSR J1741-2054, PSR J2032+4127) – X-rays: individual (Swift J174157.6-205411)

### 1. INTRODUCTION

Neutron stars hold vast stores of rotational energy. Magnetic braking in such stars generates spin-down luminosities of  $\dot{E} \approx 10^{28-38}$  erg s<sup>-1</sup>. A minute portion of this emerges in collimated coherent radio beams through which most known rotation-powered pulsars are detected. Much in pulsar electrodynamics remains obscure, including processes and locations of particle acceleration in the magnetosphere. In contrast to radio emission, pulsed gamma-ray luminosity can be a substantial fraction of  $\dot{E}$ ,

and its study therefore holds promise for significant advance in understanding magnetized rotating neutron stars.

Until recently, only six pulsars were confirmed gamma-ray emitters above 0.1 GeV (Thompson 2004). Their detection in the 1990s with the EGRET experiment on the *Compton Gamma Ray Observatory* used rotational ephemerides to fold the sparse gamma-ray photons at a known period. The ephemerides were obtained from radio observations, with the exception of Geminga, which is not a detected radio source. Given these limitations, it was not possible, for instance, to establish the fraction of gamma-ray pulsars that do not emit

<sup>20</sup> NRC Research Associate.

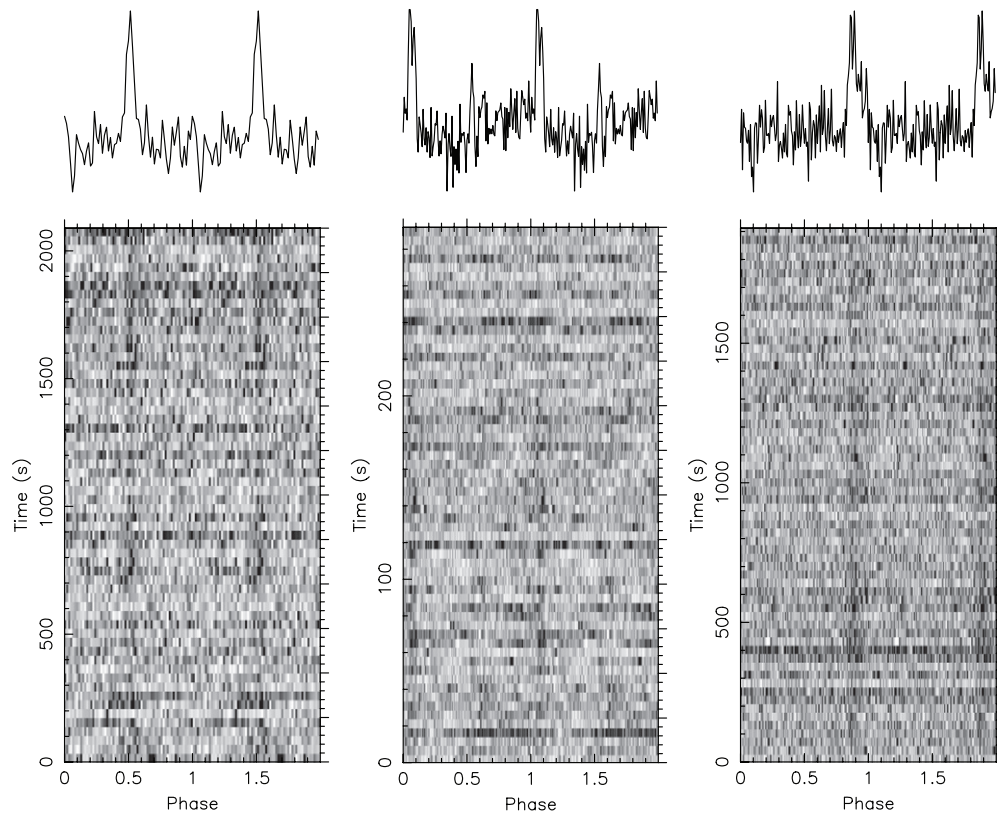


**Figure 1.** Radio detections of PSR J1741–2054: Parkes at 1.4 GHz (left), GBT at 2 GHz (center), and at 350 MHz (right). In each panel the pulse profile is shown repeated in phase, as a function of time in the grayscale, and summed at the top. The relative pulse phases between panels are arbitrary.

radio beams detectable at the Earth, i.e., that are “radio quiet.” According to predictions of outer magnetosphere models (e.g., Romani & Yadigaroglu 1995), gamma-ray beams are broader than radio beams and thus are potentially detectable from a larger solid angle. Measuring the fraction of radio-quiet gamma-ray pulsars therefore can provide information on beam shapes and emission regions, and constrain emission mechanisms (e.g., Harding et al. 2007).

The *Fermi Gamma-ray Space Telescope*, operational since mid-2008, is being used to make a torrent of pulsar discoveries with its Large Area Telescope (LAT), which has substantially greater effective area, field of view, and angular resolution than EGRET. Using radio-derived ephemerides, at least 14 pulsars have been detected for the first time by the LAT, of which eight are millisecond pulsars (Abdo et al. 2009b, 2009c, 2009g). In addition, at least 16 pulsars have been discovered in periodicity searches of gamma-ray photons (Abdo et al. 2009f). While a few of these had been searched previously in very sensitive radio observations, and therefore may be considered radio quiet (Becker et al. 2004; Halpern et al. 2004, 2007), most new LAT pulsars should be searched for radio counterparts before their true character can be determined. A radio detection yields an estimate of distance and therefore of luminosity, allowing for a more comprehensive study of these energetic neutron stars. Here we report the detection of radio pulsations, as well as additional gamma-ray and X-ray analysis, from two *Fermi* LAT pulsars.

## 2. OBSERVATIONS AND RESULTS

Nine of the new LAT pulsars are located in areas previously surveyed with the ATNF Parkes radio telescope. Three had been targeted in sensitive but unsuccessful searches (Roberts et al. 2002). We searched anew these data, as well as archival

1.4 GHz data for the other six LAT pulsars (J0633+0632, J1459–60, J1732–31, J1741–2054, J1813–1246, and J1907+06; Abdo et al. 2009f). The 95% CL error radius for these LAT sources ranged from 4′6 to 8′4. With a beam radius of 7′, there were in general multiple relevant Parkes pointings to inspect. We searched each such data set in dispersion measure (DM) with PRESTO (Ransom 2001; Ransom et al. 2002), folding time samples from the 35-minute integrations modulo the pulsar period predicted from each LAT ephemeris. In the case of PSR J1741–2054, we detected pulsations.

### 2.1. PSR J1741–2054

#### 2.1.1. Radio Measurements

The 1.4 GHz detection of the  $P = 413$  ms PSR J1741–2054 (left panel of Figure 1) is from data collected across a bandwidth of 288 MHz in the Parkes multibeam survey of the Galactic plane (e.g., Manchester et al. 2001) on 2000 November 24. This location (R.A. =  $17^{\text{h}}41^{\text{m}}51^{\text{s}}.3$ , decl. =  $-21^{\circ}01'10''$ ; all positions here refer to the J2000.0 equinox) was 7′6 away from the nominal LAT position, which had an uncertainty of 8′4 (Abdo et al. 2009c).

In order to further constrain its position, we attempted several observations of the pulsar with the NRAO Green Bank Telescope (GBT) at 2 GHz, for which the beam radius is 3′, using GUPPI<sup>21</sup> with approximately 700 MHz of usable bandwidth. We did this at six epochs, each time on a grid of pointings surrounding the nominal Parkes position. We only detected the pulsar on 2009 March 7, at R.A. =  $17^{\text{h}}41^{\text{m}}50^{\text{s}}.1$ , decl. =  $-20^{\circ}55'02''$ , 4′6 from the LAT position. The received flux varied greatly during the

<sup>21</sup> <https://wikio.nrao.edu/bin/view/CICADA/GUPPIUsersGuide>

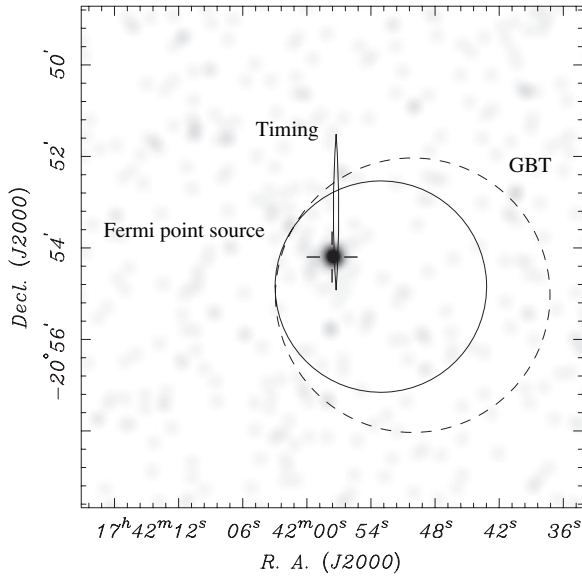


**Figure 2.** X-ray field of PSR J1741–2054: portion of *Swift* 0.2–10 keV image smoothed with a  $\sigma = 7''$  Gaussian. The soft source Swift J174157.6–205411, with 69 photons within an extraction radius of  $0'.5$ , is the only plausible counterpart in this 4.4 ks observation for PSR J1741–2054, whose  $3\sigma$  timing position (ellipse), 95% CL gamma-ray point source (solid circle), and FWHM radio (dashed circle) positional uncertainties are indicated (see Sections 2.1.2 and 2.1.4).

5-minute observation (middle panel of Figure 1), possibly due to interstellar scintillation.

We obtained from the first two detections only an upper limit on DM. We finally measured the dispersion of PSR J1741–2054 with a 350 MHz detection on March 12 (right panel of Figure 1) using the GBT BCPM (Backer et al. 1997) with a bandwidth of 48 MHz:  $DM \approx 5 \text{ pc cm}^{-3}$ . Such a low DM points to scintillation (see, e.g., Lorimer & Kramer 2005) as an explanation for the several non-detections (which further include at Parkes two observations at 1.4 GHz and one at 3 GHz, and at GBT one 0.8 GHz observation). For this DM and location at  $(l, b) = (6^\circ.42, +4^\circ.90)$ , the Cordes & Lazio (2002) electron density model yields a pulsar distance of  $d = 0.4 \text{ kpc}$ , with significant uncertainty. Hereafter, we parameterize this distance by  $d_{0.4} = d/(0.4 \text{ kpc})$ .

We have estimated the observed flux densities  $S_\nu$  for the three radio detections:  $S_{0.35} \approx 1.33 \text{ mJy}$ ,  $S_{1.4} \approx 0.16 \text{ mJy}$ , and  $S_2 \approx 0.09 \text{ mJy}$ . However, because the detection positions at the two highest frequencies are slightly offset from the true position (e.g., Figure 2), these values somewhat underestimate the flux on those days. Conversely, because of scintillation, the average flux is likely substantially lower than the position-corrected values on those days. Thus we cannot infer a spectral index.

A comparison of the barycentric pulsar periods determined from radio observations taken more than 8 yr apart implies a period derivative of  $\dot{P} = (2.7 \pm 1.1) \times 10^{-14}$  (unless otherwise noted, all uncertainties here are given at the  $1\sigma$  CL).

### 2.1.2. Gamma-ray and Radio Timing and Position

Using LAT data spanning one year, we have extracted 17 gamma-ray times of arrival (TOAs) for PSR J1741–2054 that we use to obtain a timing solution with TEMPO.<sup>22</sup> While the fitted position in R.A. has an uncertainty of only  $1''$ , that in decl. is uncertain by  $0'.6$  (see Figure 2), owing to the low ecliptic latitude

of the pulsar. In addition, a *Swift* observation reveals a probable X-ray counterpart at R.A. =  $17^{\text{h}}41^{\text{m}}57^{\text{s}}.6$ , decl. =  $-20^\circ54'11''$ , with an uncertainty of about  $4''$ . The *Swift* source position is  $5''$  in R.A. and  $58''$  in decl. from the timing position, consistent within the combined  $2\sigma$  uncertainties. Because of the still significant positional uncertainty (which should be essentially eliminated with a planned *Chandra* observation), we cannot rule out the presence of a small amount of timing noise. In any case, the timing solution already yields an accurate  $\dot{P} = 1.69 \times 10^{-14}$ . In turn,  $\tau_c = P/(2\dot{P}) = 0.39 \text{ Myr}$  and  $\dot{E} = 9.4 \times 10^{33} \text{ erg s}^{-1}$ .

We determined the position for the PSR J1741–2054 LAT point source with the binned likelihood application *ptlike*, by selecting photons above 0.125 GeV from the light curve peak, with phases  $0.24 < \phi < 0.55$  (Figure 3; this phase range subtends roughly the half-maximum level of pulsed emission, offering the best signal-to-noise ratio for localization), and varying the position to maximize the point source significance. The resulting position is R.A. =  $17^{\text{h}}41^{\text{m}}53^{\text{s}}.1$ , decl. =  $-20^\circ54'51''$ , with a 95% CL error radius of  $2'.3$ . This is only  $1/2$  away from the *Swift* source. The best radio position is also consistent with the LAT timing and *Swift* source positions (see Figure 2 for an illustration of the various positional determinations).

Using the 350 MHz and 2 GHz TOAs in a separate fit, we also obtain a higher-precision measurement of dispersion,  $DM = (4.7 \pm 0.1) \text{ pc cm}^{-3}$ . This allows the determination of the phase offset between the radio and gamma-ray pulses separately for both recent radio detections. The results are identical, and we show in Figure 3 the phase relation for the 350 MHz and gamma-ray profiles. The LAT profiles are constructed from “diffuse class” photons (Atwood et al. 2009) selected from a region with an energy-dependent radius of  $0'.8 (E/1 \text{ GeV})^{-0.75}$  (with maximum and minimum radii of  $0'.8$  and  $0'.35$ , respectively) around the best position over the time range 2008 August 4 to 2009 July 4. We used energies from 0.2 to 10 GeV. The phase alignment was done using the *gtpphase*<sup>23</sup> tool to assign phases to each LAT photon according to the best timing model. We found that the pulsed emission was well described by a three-Gaussian model and extracted the parameters with a maximum likelihood fit to the unbinned profile photon phases. We applied the model to the energy bands shown in Figure 3 (0.2–1.0 GeV and 1–10 GeV) as well as to the full (0.2–10 GeV) energy range. We found no significant difference in the widths and positions of the Gaussians, so we report here the results from a fit to the full energy range. The first gamma-ray peak (“P1”), with phase  $0.292 \pm 0.005$  and  $FWHM = 0.06 \pm 0.01$ , determines the phase offset with the radio peak,  $\delta = 0.29 \pm 0.02$ . The second gamma-ray peak (“P2”) occurs at  $\phi = 0.384 \pm 0.015$  with  $FWHM = 0.13 \pm 0.03$ , while P3 is located at  $\phi = 0.518 \pm 0.015$  with  $FWHM = 0.11 \pm 0.02$ . Interpreting the P3–P1 separation as the conventional separation in a two-peak profile yields  $\Delta = 0.226 \pm 0.016$ , although it is unclear whether this is meaningful for such a complex profile.

### 2.1.3. Gamma-ray Spectrum

To fit the gamma-ray spectrum of PSR J1741–2054, we have performed an unbinned likelihood analysis with the application *glike*<sup>23</sup>, and an additional check using the independent *ptlike*. Both approaches are outlined in Abdo et al. (2009d), and here we have used an updated instrument response function, *P6\_v3\_diff*<sup>23</sup>, that corrects a pileup effect identified in orbit. The on-axis energy resolution of the LAT is (equivalent Gaussian

<sup>22</sup> <http://www.atnf.csiro.au/research/pulsar/tempo>

<sup>23</sup> <http://fermi.gsfc.nasa.gov/ssc/data/analysis>

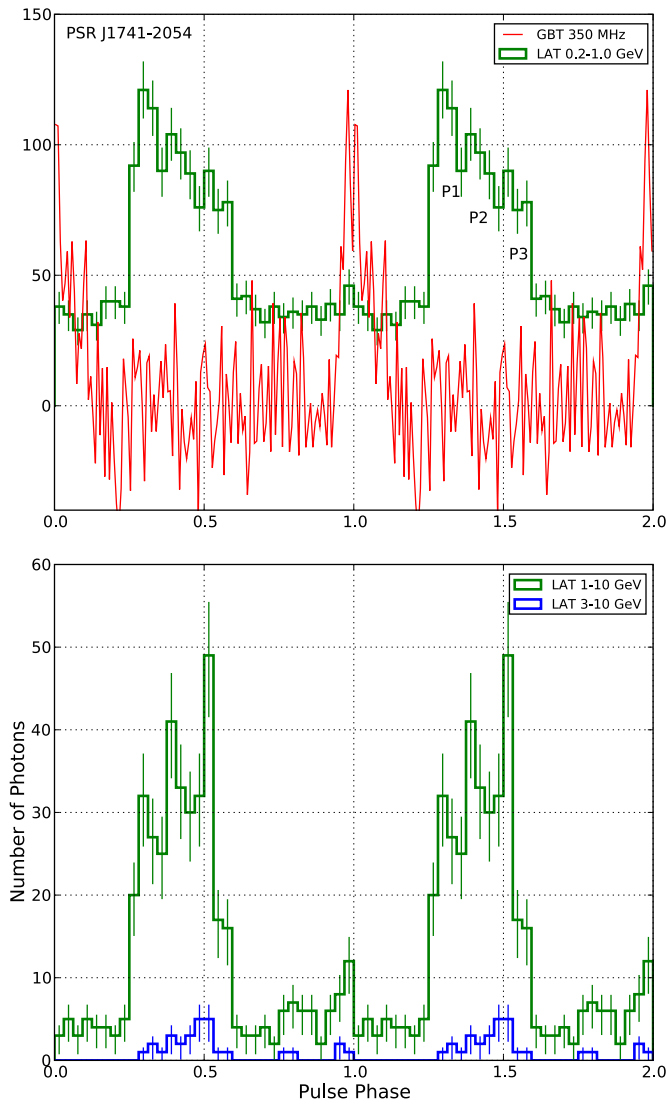


**Figure 3.** Phase-aligned *Fermi* and GBT pulse profiles of PSR J1741–2054. In the upper panel, the radio profile is displayed with an arbitrary intensity scale along with LAT counts in the 0.2–1.0 GeV band. The bottom panel shows the higher-energy LAT counts and a comparison between the two panels shows clear evolution of the peak structure (P1 weakening, P3 strengthening) with energy. At the highest energies ( $> 3$  GeV), P3 dominates. The displayed gamma-ray and radio profiles have, respectively, 32 and 128 bins per period. Two full rotations are shown.

$1\sigma$ ) 15%–9% in the 0.1–1 GeV range, 8% over 1–10 GeV, and 8%–18% in the 10–300 GeV range (Atwood et al. 2009). We used `gll_iem_v02`<sup>23</sup> as the model for the Galactic diffuse background. We selected gamma rays with energy  $> 0.1$  GeV and with zenith angle  $< 105^\circ$ , extracted from within a radius of  $15^\circ$  around the pulsar over the time range 2008 August 4 to 2009 July 4. We modeled all significant point sources in the aperture with a power-law spectrum. We found no evidence of point source emission off pulse ( $0.68 < \phi < 1.18$ ), so to increase the signal-to-noise ratio, we considered only photons with phase  $0.18 < \phi < 0.68$ . The likelihood ratio test indicates that an exponentially cutoff power law given by  $dN/dE = N_0 (E/1 \text{ GeV})^{-\Gamma} \exp(-E/E_c)$  is preferred over a simple power-law model with  $12\sigma$  significance. We find a photon index  $\Gamma = 1.1 \pm 0.1 \pm 0.2$  and a cutoff energy  $E_c = (1.0 \pm 0.1 \pm 0.2) \text{ GeV}$ , giving a photon flux above 0.1 GeV of  $(20 \pm 1 \pm 3) \times 10^{-8} \text{ cm}^{-2} \text{ s}^{-1}$  and an energy flux of  $F_\gamma =$

$(14 \pm 1 \pm 2) \times 10^{-11} \text{ erg cm}^{-2} \text{ s}^{-1}$ , where the first (second) errors indicated are statistical (systematic). The resulting gamma-ray luminosity, assuming effectively isotropic emission ( $f_\Omega = 1$ ), is  $L_\gamma = 4\pi f_\Omega F_\gamma d^2 = 2.6 \times 10^{33} d_{0.4}^2 \text{ erg s}^{-1} = 0.28 d_{0.4}^2 \dot{E}$ .

The third peak has a significantly harder spectrum than P1: it is not detectable at 0.1–0.3 GeV, then becomes gradually more significant with increasing energy, such that above 1 GeV its peak count rate exceeds that of P1. The spectrum of P2 appears to be of intermediate hardness between that of P3 and P1 (see Figure 3). The highest energy photon likely detected so far from this pulsar arrived at phase 0.491 (in P3) with energy 5.8 GeV.

#### 2.1.4. Spectrum of Likely X-ray Counterpart

The error circle of PSR J1741–2054 was observed with the *Swift* X-ray telescope on 2008 October 16, obtaining 4.4 ks of exposure with 2.5 s time sampling. The soft source Swift J174157.6–205411 near the field center is unresolved and provides 69 background-subtracted counts in the 0.3–5 keV range. There is no other detected X-ray source that is compatible with the position of the pulsar (Figure 2), and the spectral character of this source (see below) is compatible with our expectations for PSR J1741–2054. We therefore believe that Swift J174157.6–205411 is the likely pulsar counterpart.

We see no evidence in Swift J174157.6–205411 for interstellar absorption. If we fit the source spectrum with a fixed  $N_H = 1.5 \times 10^{20} \text{ cm}^{-2}$  (10 times the DM-determined free electron column), we obtain a power-law index  $\Gamma = 2.5 \pm 0.4$  and  $F_X(0.5\text{--}10 \text{ keV}) = 6.4 \times 10^{-13} \text{ erg cm}^{-2} \text{ s}^{-1}$ . Allowing  $N_H$  to vary yields  $N_H < 3 \times 10^{21} \text{ cm}^{-2}$  and a poorly determined  $\Gamma = 2.3 \pm 1.7$ . Thermal models give  $kT = (0.2 \pm 0.1) \text{ keV}$  but are not well constrained because of the unknown absorption.

The observed X-ray flux likely represents a composite spectrum similar to other relatively old and nearby gamma-ray pulsars such as Geminga and PSR B1055–52. At an age comparable to the characteristic age of PSR J1741–2054, 0.4 Myr, thermal emission from the full surface is expected to have a relatively low  $kT \approx 50\text{--}70 \text{ eV}$ . Such low temperatures alone do not reproduce the *Swift* spectrum which has significant counts above 1 keV. Thus the observed X-rays likely have a significant synchrotron component coming from secondary  $e^\pm$  pairs that are gamma-ray annihilation products.

## 2.2. PSR J2032+4127

### 2.2.1. Radio Measurements

On 2009 January 5 we used the GBT to search for radio pulsations from LAT PSR J2032+4127. We recorded data for 1 hr from an 800 MHz band centered on 2 GHz, using GUPPI to sample each of 1024 frequency channels every 0.16 ms. The telescope beam, with a radius of  $3'$ , was centered on the LAT source at R.A. =  $20^{\text{h}}32^{\text{m}}13^{\text{s}}.9$ , decl. =  $+41^\circ22'34''$  with an error radius of  $5'.1$  (Abdo et al. 2009c).

We did a search in DM while folding the data modulo the 71.6 ms period of the original LAT ephemeris, and detected the pulsar. Subsequently, we did a blind search of the radio data and established that its true period is  $P = 143 \text{ ms}$ . Following some gridding observations, we obtained an improved position: R.A. =  $20^{\text{h}}32^{\text{m}}14^{\text{s}}$ , decl. =  $+41^\circ27'00''$ , with an uncertainty radius of  $0.7$ . At this accurate position, the pulsar is clearly detectable at the GBT in only 1 minute.

We have also obtained two calibrated polarimetric observations (analyzed with PSRCHIVE; Hotan et al. 2004), one each at 2 GHz and 0.8 GHz, which show that the profile is nearly

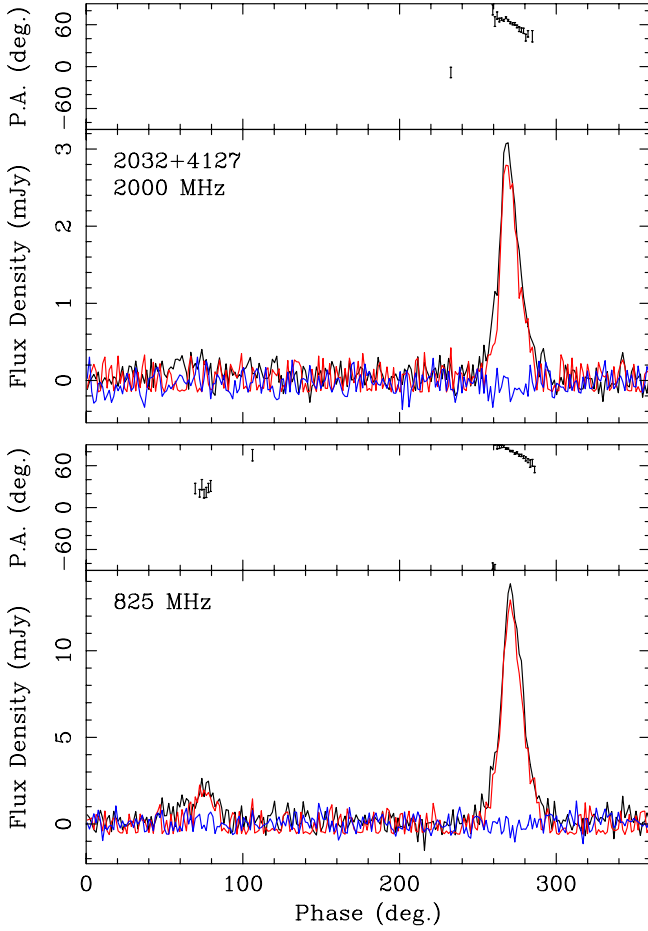


**Figure 4.** Polarimetric profiles of PSR J2032+4127 based on GBT observations with GUPPI: 0.5 hr at 2 GHz (top) and 2.0 hr at 0.8 GHz (bottom). The black traces correspond to total intensity, while the red and blue lines correspond, respectively, to linear and circular polarization. The position angles in each upper panel have been converted to the pulsar frame, using the measured  $RM = (+215 \pm 1) \text{ rad m}^{-2}$ .

100% linearly polarized, with a small interpulse detected at the lower frequency (Figure 4). The period-averaged flux density at 2 GHz is  $S_2 = 0.12 \text{ mJy}$ , and  $S_{0.8} = 0.65 \text{ mJy}$ . Each of these measurements has a fractional uncertainty of about 20%, including an allowance for the small degree of interstellar scintillation inferred from many 2 GHz observations. The resulting spectral index is  $\alpha = -1.9 \pm 0.4$ , where  $S_\nu \propto \nu^\alpha$ .

### 2.2.2. Gamma-ray and Radio Timing and Position

We are timing PSR J2032+4127 at the GBT. The measured  $DM = (114.8 \pm 0.1) \text{ pc cm}^{-3}$ , at  $(l, b) = (80^\circ 22', +1^\circ 03')$ , corresponds to  $d = 3.6 \text{ kpc}$ , according to the Cordes & Lazio (2002) model. Hereafter, we parameterize this distance by  $d_{3.6} = d/(3.6 \text{ kpc})$ . The average radio TOA uncertainty is three times smaller than the corresponding gamma-ray value, but we have a radio data span of only 6 months compared to 1 year for *Fermi*. As a consequence, the best overall timing solution is obtained from a joint fit. Some rotational instability is detectable in PSR J2032+4127 as timing noise. This is parameterized in TEMPO by the (non-stationary) second derivative of the rotation frequency,  $(-1.7 \pm 0.3) \times 10^{-21} \text{ s}^{-3}$ . The measured  $\dot{P} = 2.00 \times 10^{-14}$  implies  $\tau_c = 0.11 \text{ Myr}$  and  $\dot{E} = 2.7 \times 10^{35} \text{ erg s}^{-1}$ . The timing fit gives positional uncertainties in R.A. and decl. of  $0''.4$  and  $0''.2$ , respectively, although timing noise may contribute a systematic error amounting to  $\sim 1''$ .

Radio imaging of this region was conducted by Paredes et al. (2007) and Martí et al. (2007), including a 610 MHz survey with the Giant Metrewave Radio Telescope (GMRT), to identify potential counterparts for the very-high-energy gamma-ray source TeV J2032+4130 (Aharonian et al. 2002, 2005). Paredes et al. (2007) noted that their GMRT source 5 coincides with star 213 in the Massey & Thompson (1991, hereafter MT91) survey of massive stars in Cyg OB2, as well as with a *Chandra* X-ray source. The latter associations are explored further in Section 2.2.4. Here we conclude that PSR J2032+4127 and GMRT source 5 are one and the same based on positional coincidence (see Table 1), and because the  $(0.5 \pm 0.1) \text{ mJy}$  flux of GMRT source 5 at 610 MHz is compatible within the uncertainties with the radio spectrum of PSR J2032+4127 (Section 2.2.1). Thus, the position of PSR J2032+4127 is known to  $0''.5$  in each coordinate irrespective of timing noise. We are able to limit possible systematic uncertainties in the astrometry of the optical reference frame relative to the radio to  $\approx 0''.1$  using the Tycho position of the star Cyg OB2 4, which agrees with our optical astrometry to this level. Thus, the X-ray source coincides with the radio source and the optical star to within  $0''.6$ , which is comparable to their combined statistical and systematic uncertainties.

The timing fit also yields the phase offset between the radio and gamma-ray profiles, which is shown in Figure 5. The LAT profiles are constructed from diffuse class photons selected from a region of radius  $0''.8$  around the best position over the time range 2008 August 4 to 2009 July 4. We used only energies above 0.3 GeV to help reduce background contribution from nearby sources in this crowded field. The phase alignment was done using *gtpphase* to assign phases to each LAT photon according to the best timing model. The phase spacing between the two gamma-ray peaks ( $\Delta = 0.50 \pm 0.01$ ) and the offset between the radio and first (P1) LAT peak ( $\delta = 0.15 \pm 0.01$ ) were determined by fitting the unbinned photon phases to a two-Gaussian model.

We obtained the LAT position for PSR J2032+4127 with *plike* by selecting photons above 0.125 GeV from  $0.12 < \phi < 0.20$  and  $0.60 < \phi < 0.72$  (Figure 5), and varying the position to maximize the point source significance. The resulting R.A. =  $20^{\text{h}}32^{\text{m}}15^{\text{s}}.8$ , decl. =  $+41^\circ 26' 17''$ , with a 95% CL error radius of  $1''.7$ , is only  $1''.2$  away from the pulsar timing position.

### 2.2.3. Gamma-ray Spectrum

The Cygnus region contains several bright gamma-ray point sources and strong diffuse emission that remains difficult to model (see Figure 6). However, as with PSR J1741–2054 (Section 2.1.3), we found no evidence for point source emission off pulse, and we found that we could measure the spectrum of PSR J2032+4127 robustly by selecting only photons from on-pulse phases (defined conservatively as being  $0.08 < \phi < 0.20$  and  $0.56 < \phi < 0.80$ ). We used the same time, energy, and zenith angle cuts as for PSR J1741–2054 (Section 2.1.3), but with a  $20^\circ$  extraction radius, and modeled the bright nearby gamma-ray pulsars J2021+3651 and J2021+4026 with an exponentially cutoff power-law spectrum. We find that an exponentially cutoff power law is preferred over a simple power law with  $9\sigma$  significance. The best fit parameters,  $\Gamma = 1.1 \pm 0.2 \pm 0.2$  and  $E_c = (3.0 \pm 0.6 \pm 0.7) \text{ GeV}$ , give a photon flux above 0.1 GeV of  $(7 \pm 1 \pm 2) \times 10^{-8} \text{ cm}^{-2} \text{ s}^{-1}$  and  $F_\gamma = (9 \pm 1 \pm 2) \times 10^{-11} \text{ erg cm}^{-2} \text{ s}^{-1}$ . For assumed isotropic emission,  $L_\gamma \approx 1.4 \times 10^{35} d_{3.6}^2 \text{ erg s}^{-1} = 0.5 d_{3.6}^2 \dot{E}$ .

As with PSR J1741–2054 (Section 2.1.3), the trailing peak has a harder spectrum than P1: the P2/P1 ratio of

**Table 1**  
Source Positions Coincident with Be Star MT91 213

Source	Instrument	R.A. (J2000.0)	Decl. (J2000.0)	Reference
MT91 213	MDM 2.4 m RETROCAM	20 32 13.137(18)	+41 27 24.28(20)	This work
X-ray	<i>Chandra</i> ACIS-I	20 32 13.143(24)	+41 27 24.54(27)	This work
Radio	GMRT 610 MHz	20 32 13.092(39)	+41 27 24.16(48)	Marti et al. (2007)
PSR J2032+4127	<i>Fermi</i> LAT/GBT timing	20 32 13.07(4)	+41 27 23.4(2)	This work

**Note.** Units of right ascension are hours, minutes, and seconds, and units of declination are degrees, arcminutes, and arcseconds.

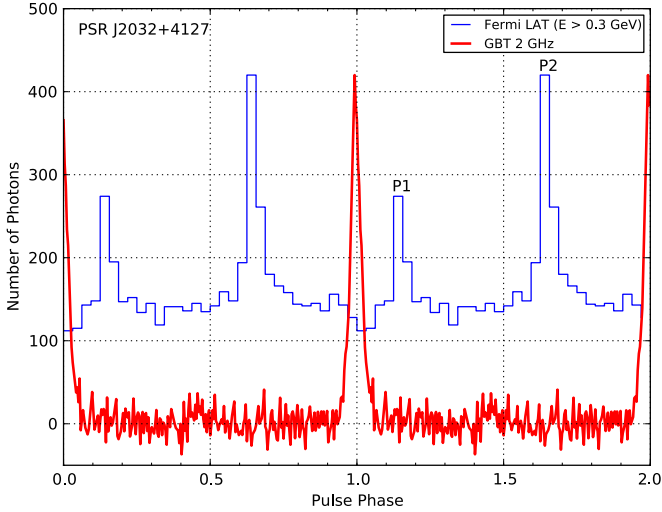


**Figure 5.** Phase-aligned GBT and *Fermi* pulse profiles of PSR J2032+4127. The gamma-ray peaks are modeled as Gaussians of, respectively,  $\text{FWHM}/P = 0.026 \pm 0.003$  and  $0.051 \pm 0.005$ . The radio profile is displayed with an arbitrary intensity scale. The radio and gamma-ray profiles are displayed with, respectively, 256 and 32 bins per period. Two full rotations are shown.

baseline-subtracted maximum count rate is 1.0 at 0.3–1 GeV but rises to 1.5 above 1 GeV, while the ratio of total counts in the peaks changes from 2.3 to 2.8 in the same energy ranges.

The highest energy photon likely detected so far from this pulsar arrived at phase 0.642 (in P2) with energy 9.8 GeV.

#### 2.2.4. X-ray and Optical Observations

PSR J2032+4127 is located in the direction of the massive Cyg OB2 stellar association. Several X-ray studies have been made of the region containing the pulsar (Butt et al. 2006; Horns et al. 2007; Mukherjee et al. 2003, 2007) to identify potential counterparts for TeV J2032+4130. Here we have reanalyzed a 50 ks *Chandra* X-ray *Observatory* archival observation of the field containing PSR J2032+4127, obtained on 2004 July 12 with a time resolution of 3.2 s (observational details can be found in Butt et al. 2006; Mukherjee et al. 2007). The pointing of this ACIS-I CCD observation placed PSR J2032+4127  $3'$  off-axis, where the angular resolution is  $\approx 1''$  FWHM. We have examined the area of the original radio gridding localization of PSR J2032+4127 (Section 2.2.1) and found several X-ray sources that are each associated with an optical counterpart; the brightest is Cyg OB2 4, an  $R = 10.2$  O7 III((f)) star (see Figure 7). Furthermore, this is a region of enhanced diffuse hard X-ray emission identified by Mukherjee et al. (2007). Figure 8 displays this  $\sim 1'$  feature and shows the timing position of PSR J2032+4127 for reference.

This area was surveyed for optical counterparts using the MDM Observatory Hiltner 2.4 m telescope on 2002 August 23 (Mukherjee et al. 2003). We compared the X-ray sources and

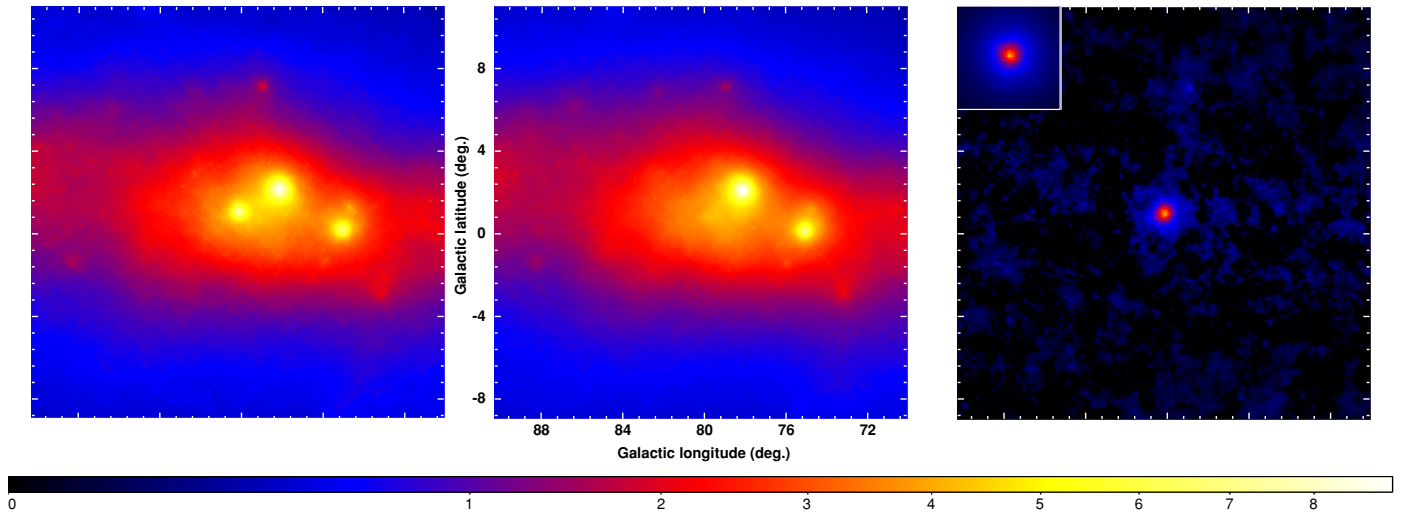


**Figure 6.** Observed *Fermi*-LAT weighted counts map of the Cygnus region ( $20^\circ \times 20^\circ$  centered on PSR J2032+4127). The photons, selected with the same time and zenith angle cuts used in the spectral analysis, and with energies between 0.2 and 10 GeV, were binned in energy and in position with a data pixel size appropriate to the point-spread function (PSF) at the measured energy. The counts in each pixel were divided by the pixel area and the integration time and then interpolated onto a  $500 \times 500$  image grid using as weights the inverse angular separation between image and data pixels out to a maximum separation equal to about 80% of the PSF. This image cube was summed over energy, and the color bar indicates the approximate rates in photons  $\text{s}^{-1} \text{sr}^{-1}$  with a square-root scale. Left: photons selected by  $0.08 < \phi < 0.20$  and  $0.56 < \phi < 0.80$  for PSR J2032+4127 (pulsar “on”). Middle: photons selected by  $0.20 < \phi < 0.56$  and  $0.80 < \phi < 1.08$  (pulsar “off”), showing the background emission, including the two bright pulsars J2021+4026 and J2021+3651. Right: on–off difference map. The only remaining source is PSR J2032+4127. The  $5^\circ \times 5^\circ$  inset shows the PSF for a source with the same spectral energy dependence as measured for PSR J2032+4127, indicating that the pulsar is consistent with a point source.

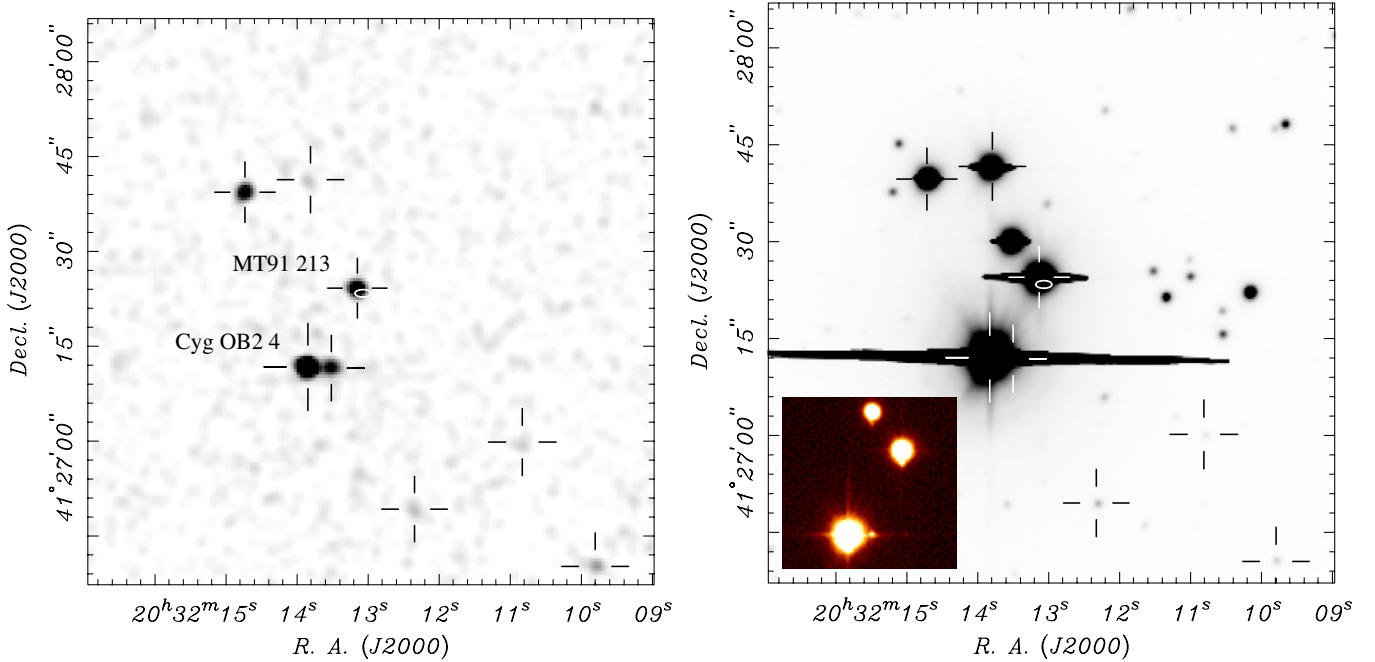


**Figure 7.** Left: portion of *Chandra* image centered on the PSR J2032+4127 timing position, shown as a  $3\sigma$  error ellipse. The *Chandra* 0.3–8 keV ACIS-I image has been exposure-corrected and smoothed with a  $0''.5$  Gaussian kernel to highlight point sources. All X-ray point sources have an identified optical counterpart, shown on the right panel, including CXOU J203213.5+412711, which is located  $3''.7$  to the west of the bright star Cyg OB2 4. The X-ray source coincident with the star MT91 213 (see Table 1) may be coming either from the star or from PSR J2032+4127. Right: an *R*-band image of the X-ray field, taken with the MDM Observatory Hiltner 2.4 m telescope. The combined exposure time is 20 minutes, and the seeing is  $1''.0$  (see Mukherjee et al. 2003 for further details). Cyg OB2 4, which masks the location of CXOU J203213.5+412711, MT91 213, and other bright stars are saturated. Locations of *Chandra* sources, astrometrically corrected using this image, are marked. The inset shows another image that was specially obtained in seeing of  $0''.6$  (see Section 2.2.4) to identify the optical counterpart of CXOU J203213.5+412711,  $3''.7$  to the west of Cyg OB2 4.

their optical counterparts in Figure 7 to register the X-ray image with a correction of  $-0''.16$  in R.A. and  $+0''.31$  in decl. for the X-ray sources. Thus, we confirm that an X-ray source coincides with the radio position of PSR J2032+4127/GMRT 5 and the star MT91 213 to within  $<0''.6$ , as listed in Table 1.

MT91 indicate a spectral type B0 Vp and  $V = 11.95$  for star 213. We obtained a spectrum of MT91 213 on 2009 June 13 using the MDM 2.4 m telescope with Modspec, covering the wavelength range 4220–7550 Å at 4 Å resolution. Figure 9 shows the red portion of the spectrum, where emission lines of H $\alpha$  and He I are evident. The equivalent width of H $\alpha$  is  $-12.6$  Å, and the He I lines have asymmetric peaks that are separated by  $\approx 500$  km s $^{-1}$ , properties that are typical of Be stars.

Since their spectra covered only the blue region, where emission lines are not obvious, MT91 did not report a Be classification for star 213. Instead, they remarked that the absorption lines appear unusually broad, and concluded that the star is multiple, thus the peculiar classification. Since all of the absorption lines in our spectrum are filled in with emission, we have no additional evidence to support the suggestion that MT91 213 is a multiple system. In addition, Kiminki et al. (2007) did not find any evidence for binary motion among 10 spectra of MT91 213 obtained between 1999 and 2004. Massey & Thompson (1991) derive a color excess  $E(B - V) = 1.43$  for star 213, corresponding to  $A_V = 4.28$ . This optical extinction would translate to X-ray column density  $N_H = 7.7 \times 10^{21}$  cm $^{-2}$  using the conversion of Predehl & Schmitt (1995). We performed spectral fits to the 83 X-ray photons detected from this source by *Chandra*. Power-law and Raymond–Smith plasma models fit equally well, with photon index  $\Gamma = 2.1 \pm 0.7$  and  $kT = 4^{+9}_{-2}$  keV, respectively. The fitted  $N_H$  is consistent with the optical extinction to MT91 213. The

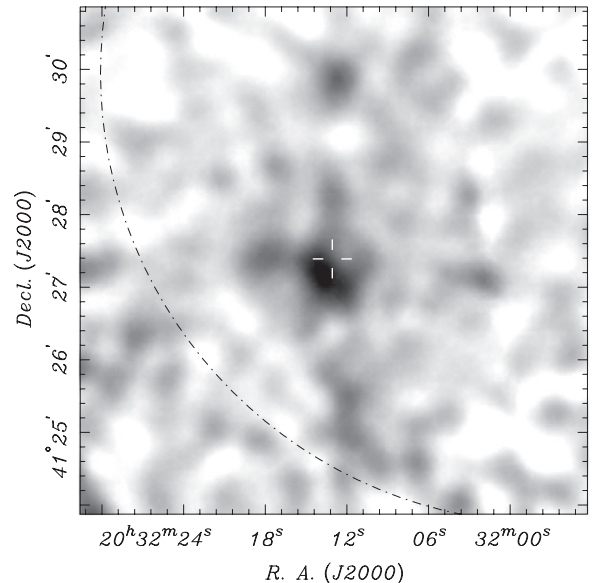


**Figure 8.** Diffuse X-ray emission in the vicinity of PSR J2032+4127. The point sources have been removed from the *Chandra* 0.3–8 keV ACIS-I image of Figure 7, which is exposure-corrected and smoothed with a Gaussian kernel of  $\sigma = 14''$  to highlight diffuse emission. This image is a  $7' \times 7'$  zoom-in on Figure 3 from Mukherjee et al. (2007). The cross is located at the pulsar timing position (see Figure 7). The dot-dashed circle approximates the extent of the HEGRA source TeV J2032+4130.

unabsorbed X-ray flux in the 0.5–10 keV band is  $F_X \approx 3.2 \times 10^{-14}$  erg cm $^{-2}$  s $^{-1}$  for the power law. The corresponding luminosity is  $L_X \approx 1.1 \times 10^{31} d_{1.7}^2$  erg s $^{-1}$ .

Paredes et al. (2007) suggested that the radio and X-ray sources coincident with MT91 213 are produced in a colliding

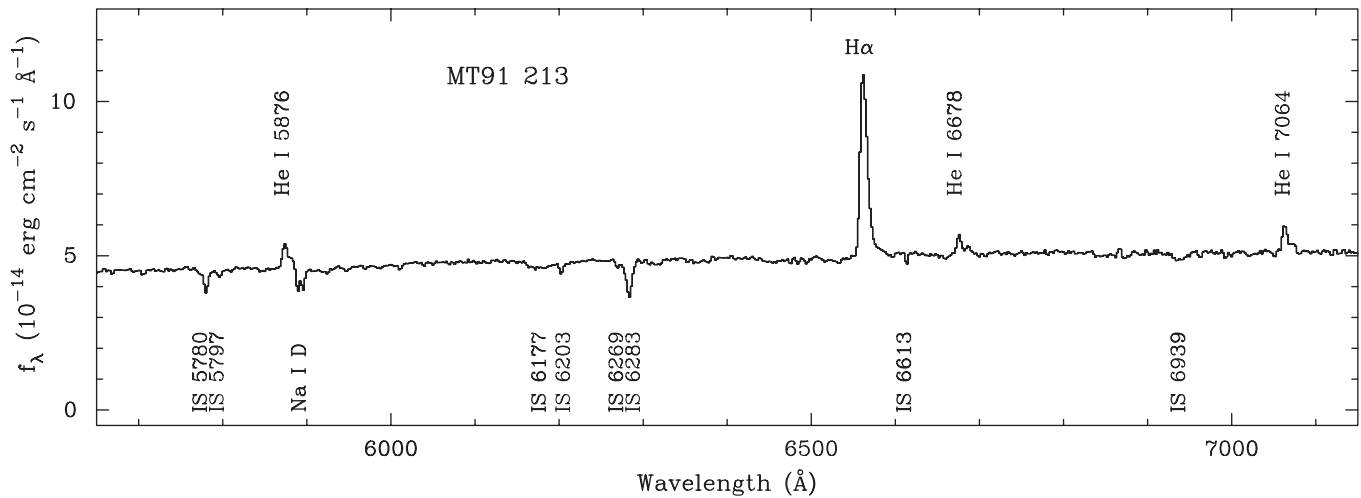


**Figure 9.** Portion of the optical spectrum of MT91 213, showing emission lines that are typical of Be stars. The equivalent width of  $H\alpha$  is  $-12.6 \text{ \AA}$ , and the He I lines have asymmetric peaks that are separated by  $\approx 500 \text{ km s}^{-1}$ . Interstellar absorption lines are marked below the spectrum.

wind binary. While we now know that the radio source is a pulsar, it is not clear what the relationship is between the radio pulsar, the X-ray source, and the Be star. The pulsar lacks any evidence of binary motion in its timing. The kinematic contribution to the pulsar’s frequency derivatives from its acceleration in orbit around a  $M_c \sim 20 M_\odot$  companion (neglecting orbital eccentricity) would be

$$\left| \frac{\dot{f}_k}{f} \right| < 1.2 \times 10^{-13} \left( \frac{P_{\text{orb}}}{100 \text{ yr}} \right)^{-4/3} \left( \frac{M_c}{20 M_\odot} \right)^{1/3} \sin i \text{ s}^{-1},$$

$$\left| \frac{\ddot{f}_k}{f} \right| < 3.2 \times 10^{-22} \left( \frac{P_{\text{orb}}}{100 \text{ yr}} \right)^{-7/3} \left( \frac{M_c}{20 M_\odot} \right)^{1/3} \sin i \text{ s}^{-2}.$$

From Table 2, we obtain  $\dot{f}/f = -1.4 \times 10^{-13} \text{ s}^{-1}$  and  $\ddot{f}/f = -2.4 \times 10^{-22} \text{ s}^{-2}$ . If the pulsar is a binary companion of the Be star, the orbital period is probably  $P_{\text{orb}} \geq 100 \text{ yr}$  in order not to exceed these observed limits on the pulsar’s acceleration.

Such long-period systems are not known to exist (the longest is 5 yr), presumably because such a wide binary would not survive the supernova kick. Instead, the pulsar is probably superposed by chance on the position of the star in this crowded field, in which case the X-ray source may belong either to the radio pulsar or to the Be star, or both. The degraded PSF at the off-axis location of the *Chandra* image does not allow us to resolve this question. But the X-ray luminosity of the source is a fraction  $\sim 4 \times 10^{-5} d_{1.7}^2$  of the pulsar’s  $\dot{E}$ , which is within the range of observed efficiencies of young pulsars (e.g., Camilo et al. 2006). It is also compatible with the X-ray luminosities of single early Be stars, although on the high end (Berghöfer et al. 1997; Cohen et al. 1997).

For completeness, we note that the location of one X-ray source that lies  $3''.7$  to the west of Cyg OB2 4, CXOU J203213.5+412711, was saturated in all of our optical images, as shown in the right main panel of Figure 7. Its corrected coordinates are R.A. =  $20^{\text{h}}32^{\text{m}}13^{\text{s}}.50$ , decl. =  $+41^\circ27'11''.8$ , with an error radius of  $\approx 0''.3$ . We investigated the nature of this source because it is the only other hard X-ray source (with half of the 55 detected photons above 2 keV) close to the pulsar timing position.

To identify CXOU J203213.5+412711 it was necessary to obtain an unsaturated optical image in good seeing. Images of 1 s exposure were acquired on the MDM 2.4 m telescope

on 2009 May 24 using RETROCAM (Morgan et al. 2005) and the Sloan Digital Sky Survey (SDSS)  $r$  filter in seeing of  $0''.6$ . The inset of Figure 7 (right) is the sum of 12 such exposures, which clearly reveals a star to the west of Cyg OB2 4 that we measure to fall within  $0''.3$  of the position of CXOU J203213.5+412711. On 2009 May 25, we obtained an optical spectrum of this star on the MDM 2.4 m telescope, using a  $1''$  wide slit that cleanly isolated it. The resulting spectrum is that of a Be star, with an  $H\alpha$  emission line as well as H and He absorption.

The optical spectra of CXOU J203213.5+412711 and Cyg OB2 4 obtained on the same night show interstellar absorption features that can be used to assess their relative distances. The equivalent widths of the features agree to within  $\sim 15\%$ , comparable to their uncertainties, which implies that CXOU J203213.5+412711 is probably located in the Cyg OB2 association. There are too few X-ray counts from CXOU J203213.5+412711 to obtain a spectrum, but we can estimate its flux by assuming an absorbed power-law model. Massey & Thompson (1991) derive a color excess  $E(B - V) = 1.59$  for Cyg OB2 4 corresponding to  $A_V = 4.50$ . This optical extinction would translate to X-ray column density  $N_{\text{H}} = 8 \times 10^{21} \text{ cm}^{-2}$  using the conversion of Predehl & Schmitt (1995). Assuming this  $N_{\text{H}}$  and  $\Gamma = 2.0$ , the unabsorbed flux of CXOU J203213.5+412711 in the 0.5–10 keV band is  $F_X \approx 2.5 \times 10^{-14} \text{ erg cm}^{-2} \text{ s}^{-1}$ . The corresponding luminosity is  $L_X \approx 9 \times 10^{30} d_{1.7}^2 \text{ erg s}^{-1}$ . X-ray luminosities of Be stars decline sharply from early to late spectral type (Berghöfer et al. 1997; Cohen et al. 1997). The optical faintness of this star would seem to indicate a late spectral type. More precise spectral classification of CXOU J203213.5+412711 is needed to evaluate whether its high X-ray luminosity is anomalous. In any case, it is the second Be star discovered in the vicinity of PSR J2032+4127 that is apparently not connected to it. Curiously, this star and Cyg OB2 4 are both closer to the centroid of the diffuse emission in Figure 8 than is PSR J2032+4127, even though that may not have any physical significance.

### 3. DISCUSSION

With the detection of radio pulsations from two of the 16 pulsars recently discovered in blind searches of *Fermi*-LAT gamma-ray photons (Abdo et al. 2009f), we have taken a

**Table 2**  
Measured and Derived Parameters for PSRs J1741–2054 and J2032+4127

Parameter	PSR J1741–2054	PSR J2032+4127
Right ascension, R.A. (J2000.0) <sup>a</sup>	17 <sup>h</sup> 41 <sup>m</sup> 57 <sup>s</sup> .27(8)	20 <sup>h</sup> 32 <sup>m</sup> 13 <sup>s</sup> .07(4)
Declination, decl. (J2000.0) <sup>a</sup>	−20°53′13(34)′′	+41°27′23′.4(2)′′
Galactic longitude, $l$ (deg.)	6.42	80.22
Galactic latitude, $b$ (deg.)	+4.90	+1.03
Spin period, $P$ (s)	0.41369996385(6)	0.14324743146(2)
Period derivative, $\dot{P}$ ( $10^{-14}$ )	1.694(3)	2.0063(1)
Epoch (MJD)	54826.0	54840.0
Timing data span (MJD)	54647–55004	54647–55033
Timing residual, rms (ms)	3.4	0.36
Dispersion measure, DM ( $\text{pc cm}^{-3}$ )	4.7(1)	114.8(1)
Rotation measure, RM ( $\text{rad m}^{-2}$ )	...	$215 \pm 1$
Flux density at 2 GHz, $S_2$ (mJy)	... <sup>b</sup>	$0.12 \pm 0.03$
Radio–gamma-ray profile offset, $\delta$ ( $P$ )	$0.29 \pm 0.02$	$0.15 \pm 0.01$
Gamma-ray profile peak-to-peak separation, $\Delta$ ( $P$ )	$0.23 \pm 0.02$ <sup>c</sup>	$0.50 \pm 0.01$
Gamma-ray ( $> 0.1$ GeV) photon index, $\Gamma$	$1.1 \pm 0.1 \pm 0.2$	$1.1 \pm 0.2 \pm 0.2$
Gamma-ray cutoff energy, $E_c$ (GeV)	$1.0 \pm 0.1 \pm 0.2$	$3.0 \pm 0.6 \pm 0.7$
Photon flux ( $> 0.1$ GeV) ( $10^{-8} \text{ cm}^{-2} \text{ s}^{-1}$ )	$20 \pm 1 \pm 3$	$7 \pm 1 \pm 2$
Energy flux ( $> 0.1$ GeV), $F_\gamma$ ( $10^{-11} \text{ erg cm}^{-2} \text{ s}^{-1}$ )	$14 \pm 1 \pm 2$	$9 \pm 1 \pm 2$
Spin-down luminosity, $\dot{E}$ ( $\text{erg s}^{-1}$ )	$9.4 \times 10^{33}$	$2.7 \times 10^{35}$
Characteristic age, $\tau_c$ (Myr)	0.39	0.11
Surface dipole magnetic field strength ( $10^{12}$ G)	2.7	1.7
Distance, $d$ (kpc) <sup>d</sup>	0.4	3.6

**Notes.** Values in parentheses are nominal TEMPO uncertainties on the last digit for parameters determined in timing fits. For gamma-ray spectral parameters, the first uncertainty is statistical and the second accounts for systematics.

<sup>a</sup> The decl. of PSR J1741–2054 is known with greater precision than from this timing fit from a *Swift* observation (see Figure 2). In the timing fit for PSR J2032+4127 we account for rotational instability in the pulsar, parameterized by the second derivative of spin frequency:  $\ddot{f} = -1.7(3) \times 10^{-21} \text{ s}^{-3}$ .

<sup>b</sup> The flux density received from PSR J1741–2054 varies greatly at 1.4 GHz and 2 GHz, due to interstellar scintillation (see Section 2.1.1).

<sup>c</sup> This is the separation between P1 and P3 (see Figure 3).

<sup>d</sup> Distances are estimated from the DM and the electron density model of Cordes & Lazio (2002). PSR J2032+4127 may be located at approximately half of this distance (see Section 3.2).

further step toward inferring the fraction of radio-quiet gamma-ray-emitting pulsars. Our non-detection of radio pulsations from eight other LAT pulsars (Section 2) is not constraining enough, owing to insufficient sensitivity: minimum detectable flux densities were  $S_{1.4} \sim 0.06$  mJy for the three observed by Roberts et al. (2002) and  $S_{1.4} \sim 0.2$  mJy for the remaining five, while very young radio pulsars have luminosities at least as low as  $L_{1.4} \equiv S_{1.4}d^2 \approx 0.5$  mJy kpc<sup>2</sup> (Camilo et al. 2002), and the smallest measured pulsar luminosity is  $L_{1.4} \approx 0.02$  mJy kpc<sup>2</sup> (see Deller et al. 2009).

The *Fermi* LAT bright source list (Abdo et al. 2009c) catalogs the 205 most significant sources above 0.1 GeV. Due to the spatially varying Galactic background, this is not a flux-limited sample, but we consider it here as a crude proxy for an unbiased sample containing a substantial number of pulsars.

A total of 30 known pulsars are represented in the list, including 15 discovered blindly in LAT data. We exclude from consideration here three (previously known) millisecond pulsars, since millisecond pulsars could have different emission properties. Of the remaining 27 pulsars, 13 are already known radio emitters, including the two reported here. Four others can be considered to be radio quiet based on previous searches (see Becker et al. 2004; Halpern et al. 2004, 2007; Kassim & Lazio 1999). The status of the remaining 10 is still unclear, but given our success with PSRs J1741–2054 and J2032+4127, it is reasonable to suppose that some will eventually be detected in

the radio. Therefore, among presently identified pulsars in the LAT bright source list (Abdo et al. 2009c),  $\geq 50\%$  emit radio pulsations.

In addition, however, nearly 50 of the 205 bright LAT sources are good pulsar candidates (they are without known active galactic nucleus (AGN) associations and are not variable). Regardless of whether gamma-ray pulsations can be detected from these, most of them are likely to be gamma-ray pulsars. Thus, in order to determine the true fraction of radio-quiet gamma-ray pulsars, it is crucial to do sufficiently sensitive radio searches of most of these 50 unidentified gamma-ray sources.

We now discuss PSRs J1741–2054 and J2032+4127 in turn, for which we have gathered many of the measured and derived parameters in Table 2.

### 3.1. PSR J1741–2054

The average radio flux density of PSR J1741–2054 is uncertain due to scintillation, but given our one detection at 1.4 GHz, the average luminosity is  $L_{1.4} < 0.025 d_{0.4}^2$  mJy kpc<sup>2</sup>, which is the smallest of any detected radio pulsar. Scintillation, which makes it difficult to observe this pulsar, is a result of the very small DM and thus small distance. At  $\sim 5$  times the distance (still at only  $\sim 2$  kpc), a pulsar of such luminosity would not be detectable with any existing telescope. This is worth considering when discussing “radio-quiet” neutron stars.

There are only eight pulsars known with DM smaller than that of PSR J1741–2054 (see Manchester et al. 2005).<sup>24</sup> Two of them are exceedingly bright, and were discovered more than 40 years ago. Four others are millisecond pulsars, for which such a small DM is relatively easy to distinguish from zero in searches, and thus from terrestrial radio interference. Only the remaining two were discovered in modern searches (Tauris et al. 1994; Young et al. 1999). Thus, while very nearby pulsars are intrinsically rare, it is also the case that they have proven difficult to detect in radio surveys, with implications for the completeness of the known sample.

PSR J1741–2054 was detected by EGRET as 3EG J1741–2050 (Hartman et al. 1999). Its EGRET flux above 0.1 GeV is similar to the LAT flux (Section 2.1.3). With  $P = 413$  ms,  $\tau_c = 0.39$  Myr, and  $d \approx 0.4$  kpc, PSR J1741–2054 is reminiscent of the nearest middle-aged pulsars, Geminga ( $P = 237$  ms,  $\tau_c = 0.34$  Myr,  $d = 0.25$  kpc) and PSR B0656+14 ( $P = 384$  ms,  $\tau_c = 0.11$  Myr,  $d = 0.29$  kpc), although it has only 1/4 of their spin-down luminosity.

Among the known population of young (non-millisecond) pulsars, PSR J1741–2054 has one of the smallest gamma-ray peak separations ( $\Delta = 0.23$ ) and largest gamma-ray–radio lags ( $\delta = 0.29$ ). Together, these values are roughly in agreement with the expectation from “outer-gap” (OG) gamma-ray beam models, which predict an inverse dependence of  $\Delta$  on  $\delta$  (e.g., Romani & Yadigaroglu 1995). In OG models these parameters depend principally on the viewing angle  $\zeta$  (measured from the rotation axis of the pulsar). For PSR J1741–2054, the measured ( $\Delta$ ,  $\delta$ ) indicate a smaller  $\zeta$  than for most other known gamma-ray pulsars. In detail, however, basic geometric models still cannot explain many of the observed ( $\Delta$ ,  $\delta$ ), including for PSR J1741–2054, let alone features like the three peaks identified in this pulsar (Figure 3 and Section 2.1.2), and further ingredients are likely needed (see Watters et al. 2009).

In order to compute the flux of a gamma-ray pulsar averaged over the sky, we need to know the geometry-dependent “beaming” factor  $f_\Omega$  that corrects the phase-averaged flux measured by *Fermi*. It is still not possible to infer this precisely for a given pulsar, especially when we do not possess independent geometric information (such as from radio pulsar polarization measurements or from high-resolution X-ray observations of pulsar wind nebulae (PWNe)). Nevertheless, most promising models, which in addition to OG include “two-pole caustic” (TPC) models (Dyks & Rudak 2003), predict large  $f_\Omega$ . For the observed profile characteristics of PSR J1741–2054, which resemble somewhat those of PSR B1706–44 (Pellizzoni et al. 2009), the OG and TPC models appear to suggest that  $f_\Omega \approx 0.5$ –1 (Watters et al. 2009).

Based on the *Fermi* spectral parameters reported in Section 2.1.3 for PSR J1741–2054, we obtain  $L_\gamma(> 0.1 \text{ GeV}) = 4\pi f_\Omega F_\gamma d^2 = 2.6 \times 10^{33} f_\Omega d_{0.4}^2 \text{ erg s}^{-1} = 0.28 f_\Omega d_{0.4}^2 \dot{E}$ . Plausibly  $f_\Omega \approx 0.5$ –1, which might eventually be improved with further modeling, and  $d_{0.4} \approx 1$ . PSR J1741–2054, which has the smallest  $\dot{E}$  of any established non-millisecond gamma-ray pulsar, has a high inferred efficiency for converting spin-down luminosity into gamma rays,  $\eta \equiv L_\gamma/\dot{E} = 0.28 f_\Omega d_{0.4}^2$ . This is in line with the trend that  $\eta$  increases with decreasing  $\dot{E}$  (Thompson et al. 1999). Constraining the distance with very long baseline interferometry (VLBI) measurements will be difficult, owing to the very small flux, but the proper motion could be accessible via either VLBI or

*Hubble Space Telescope* measurements. Sensitive X-ray observations will also prove very useful in constraining the properties of this neutron star (see Section 2.1.4).

Non-millisecond gamma-ray pulsars typically have observed pulse profiles with two distinct peaks. In many such cases, the trailing peak has a harder spectrum than P1. Although PSR J1741–2054 appears to have three distinct peaks, it follows this trend in that its trailing peak has a harder spectrum (see Section 2.1.3). One respect in which PSR J1741–2054 appears to stand out from non-millisecond pulsars is in having the smallest spectral cutoff energy reported so far,  $E_c = 1.0$  GeV. It remains to be determined whether this portends an incipient trend.

### 3.2. PSR J2032+4127

The radio luminosity of PSR J2032+4127, scaled to the standard frequency of 1.4 GHz using its estimated spectral index (Section 2.2.1), is  $L_{1.4} = 3 d_{3.6}^2 \text{ mJy kpc}^2$ . While  $\sim 100$  times larger than that of PSR J1741–2054, this is still a small luminosity among the observed young pulsar population (see, e.g., Camilo et al. 2009). The actual distance to the pulsar may differ significantly from the 3.6 kpc estimated from the DM (Cordes & Lazio 2002). As we argue below, it may be that  $d_{3.6} \approx 0.5$ .

As shown in Figure 4, we have made polarimetric observations of PSR J2032+4127, and have measured Faraday rotation amounting to rotation measure  $\text{RM} = +215 \text{ rad m}^{-2}$ . This implies an average Galactic magnetic field along the line of sight, weighted by the free electron density, of  $2.3 \mu\text{G}$ , which is a typical Galactic value. There are very few pulsars with measured RM in the approximate direction of this pulsar (Han et al. 2006; Abdo et al. 2009a), so that this measurement cannot be put into context and it does not provide a constraint on the pulsar distance. Also, we have tried to obtain information on the pulsar geometry by fitting a “rotating vector model” (Radhakrishnan & Cooke 1969) to the swing with pulse phase of the position angle of linear polarization (PA; top sub-panels of Figure 4). Unfortunately the fits are unconstrained, because of the limited longitude coverage and relatively shallow PA swing. The radio profile of PSR J2032+4127 appears similar to those of several young pulsars in being simple, relatively narrow, highly linearly polarized, and in having little variation in PA (see Johnston & Weisberg 2006; Weltevrede & Johnston 2008).

The gamma-ray profile of PSR J2032+4127 (Figure 5) is broadly similar to those of several young pulsars, such as PSRs J2021+3651 (Abdo et al. 2009a; Halpern et al. 2008) and J0205+6449 (Abdo et al. 2009b). It has two narrow gamma-ray peaks preceded by the radio pulse, with  $(\Delta, \delta) = (0.50, 0.15)$ . These values can be approximately understood within the context of both the OG and the TPC beam models. In detail, however,  $\delta$  is somewhat larger than expected for the observed  $\Delta$ , given the simplest geometric models (see Watters et al. 2009). This interpretive problem arises as well for PSRs J2021+3651 and J0205+6449. Unlike for PSR J1741–2054, these ( $\Delta$ ,  $\delta$ ) indicate a large viewing angle  $\zeta$  for PSR J2032+4127, and a broad fan-like beam with a correction factor  $f_\Omega \approx 1$ .

Based on the spectrum of PSR J2032+4127 (Section 2.2.3), we obtain  $L_\gamma(> 0.1 \text{ GeV}) \approx 1.4 \times 10^{35} f_\Omega d_{3.6}^2 \text{ erg s}^{-1}$ . With  $f_\Omega \approx 1$  as indicated above,  $\eta \approx 0.5 d_{3.6}^2$ . This is a very large nominal efficiency for a pulsar with  $\dot{E} = 2.7 \times 10^{35} \text{ erg s}^{-1}$ , which has an open field line voltage of  $10^{15} \text{ V}$  (cf. Arons 1996). Part of the answer may lie in a smaller distance, and indeed it is plausible that  $d_{3.6} \approx 0.5$  (see Section 3.2.1).

<sup>24</sup> <http://www.atnf.csiro.au/research/pulsar/psrcat>

PSR J2032+4127 is located in the Cygnus region, which contains several bright gamma-ray point sources and strong spatially varying diffuse emission. This leads to particular difficulty in modeling the spectrum of the pulsar (see Section 2.2.3 and Figure 6). In the *Fermi* bright source list (Abdo et al. 2009c), PSR J2032+4127 corresponds to the source 0FGL J2032.2+4122, which has a flux of  $(54 \pm 5) \times 10^{-8} \text{ cm}^{-2} \text{ s}^{-1}$ . In Section 2.2.3, however, we have reported for PSR J2032+4127 a flux of  $(7 \pm 1 \pm 2) \times 10^{-8} \text{ cm}^{-2} \text{ s}^{-1}$ , or about 1/8 of that given for 0FGL J2032.2+4122. Compared to Abdo et al. (2009c), we have used significantly more data, an updated LAT response function, an improved diffuse background model, considered only on-pulse emission (see Sections 2.2.3 and 2.1.3), and modeled additional point sources in the field. Finally, the Abdo et al. (2009c) spectral model was a simple power law, generally inadequate to describe the spectral breaks found in pulsars. Together, these differences presumably account for the large discrepancy in photon flux. The new, much smaller, flux value nevertheless implies an unreasonably large efficiency  $\eta \approx 0.5 d_{3.6}^2$ . We believe that for PSR J2032+4127 our flux estimate is the most reliable one available at this point, but still subject to improvement as the modeling of the complex Cygnus region evolves. And we also suggest that a reasonable conversion efficiency for PSR J2032+4127 is most naturally achieved with  $d_{3.6} \approx 0.5$ .

The trailing peak of PSR J2032+4127 has a harder spectrum than P1 (Section 2.2.3). This behavior is similar to that observed in PSRs J2021+3651 and J0205+6449 (Abdo et al. 2009a, 2009b), which as already noted have pulse profiles broadly similar to PSR J2032+4127, but have  $\dot{E}$  that are larger by factors of 10 and 100, respectively. This gathering trend now applies to many known gamma-ray pulsars with distinct peaks, from PSR J1741–2054 (Section 2.1.3) to the Crab (Thompson 2001), spanning a factor of 5000 in  $\dot{E}$ .

### 3.2.1. The (Formerly) Unidentified TeV J2032+4130

TeV J2032+4130 was discovered serendipitously by the HEGRA system of Atmospheric Cherenkov Telescopes in observations of the Cygnus region over the period 1999–2001 (Aharonian et al. 2002). It was the first unclassified TeV source, and its origin remained undetermined until now. Analysis of combined HEGRA data from 1999–2002 gave a final position centroid for the extended TeV source of R.A. =  $20^{\text{h}}31^{\text{m}}57^{\text{s}}.0 \pm 6^{\text{s}}.2_{\text{stat}} \pm 13^{\text{s}}.7_{\text{sys}}$ , decl. =  $+41^{\circ}29'57'' \pm 1'.1_{\text{stat}} \pm 1'.0_{\text{sys}}$ , and a Gaussian radius of  $\sigma = 6'.2 \pm 1'.2_{\text{stat}} \pm 0'.9_{\text{sys}}$  (Aharonian et al. 2005). The HEGRA-measured photon flux above 1 TeV is  $(6.9 \pm 1.8) \times 10^{-13} \text{ cm}^{-2} \text{ s}^{-1}$  with  $\Gamma = 1.9 \pm 0.3$ . MAGIC detected TeV J2032+4130 at a best position of R.A. =  $20^{\text{h}}32^{\text{m}}20^{\text{s}} \pm 11^{\text{s}}_{\text{stat}} \pm 11^{\text{s}}_{\text{sys}}$ , decl. =  $+41^{\circ}30'36'' \pm 1'.2_{\text{stat}} \pm 1'.8_{\text{sys}}$ , and radius  $\sigma = 6'.0 \pm 1'.7_{\text{stat}} \pm 0'.6_{\text{sys}}$  (Albert et al. 2008). The flux measured by MAGIC above 1 TeV is  $4.5 \times 10^{-13} \text{ cm}^{-2} \text{ s}^{-1}$  with photon index  $\Gamma = 2.0 \pm 0.3$ . The Whipple Observatory detected a source of luminosity  $L_{\gamma} = 4 \times 10^{33} d_{1.7}^2 \text{ erg s}^{-1}$ , assuming a Crab-like spectrum (Konopelko et al. 2007), which is about a factor of 2 greater than that measured by HEGRA, but probably consistent given the uncertainty in the spectrum. The Whipple position and extent of the source are marginally consistent with those of HEGRA. Milagro detects a diffuse source in a  $3^{\circ} \times 3^{\circ}$  region centered on TeV J2032+4130, that exceeds the HEGRA flux by a factor of 3 (Abdo et al. 2007). This region may contain multiple sources; the Milagro excess at the location of the pulsar is  $7.6 \sigma$  (Abdo et al. 2009e) and is consistent with an extrapolation of the HEGRA spectrum. None of the experiments have found strong

evidence for flux variability of TeV J2032+4130 in the period 1999–2005.

Pulsar wind nebulae comprise the largest class of Galactic TeV sources,<sup>25</sup> and all but the youngest, with ages of  $\sim 10^3$  yr, are spatially extended. PSR J2032+4127 is located within the  $1 \sigma$  extent of TeV J2032+4130 (see Figure 8), only  $4'$  from its HEGRA centroid. We therefore propose its PWN as the source of TeV J2032+4130. Further support for the association of PSR J2032+4127 with TeV J2032+4130 comes from comparing their properties with those of other TeV PWNe.

First, however, we discuss the implications of the apparent coincidence of PSR J2032+4127 with the massive young star cluster Cyg OB2. Distance estimates to Cyg OB2 range over 1.45–1.7 kpc (Hanson 2003; Massey & Thompson 1991), while the nominal DM distance of PSR J2032+4127 is 3.6 kpc. Considering the possibility of unmodeled local enhancements in the electron density that may cause the DM model to overestimate the pulsar distance, we do not rule out that PSR J2032+4127 could be colocated with Cyg OB2 (which, as noted in Section 3.2, would imply a far more reasonable pulsar GeV conversion efficiency  $\eta$ ). PSR J2032+4127 is projected  $15'$  from the center of the cluster, which has a half-light radius of  $13'$  and a diameter of  $\sim 2^{\circ}$  as determined from Two Micron All Sky Survey (2MASS) star counts (Knödseder 2000).

Conventional wisdom holds that no neutron stars have been born in Cyg OB2 because the age of the majority of its stars, determined from isochrone fitting, is only 2–2.5 Myr (Hanson 2003; Negueruela et al. 2008). At this age, stars of  $M < 35 M_{\odot}$  are still close to the main sequence, and no supernovae have occurred. However, there is evidence for earlier episodes of star formation in the immediate neighborhood, such as the  $\sim 5$ –7 Myr-old A stars discovered by Drew et al. (2008) within a  $1^{\circ}$  radius of Cyg OB2 and at the same distance. Older OB stars coincident with Cyg OB2 are also discussed by Hanson (2003). Therefore, we cannot rule out that the progenitor star of PSR J2032+4127 was born in a recent episode of star formation at the same distance as Cyg OB2, while the typical neutron star velocity of  $\sim 250 \text{ km s}^{-1}$  would allow it to have traveled  $\sim 1^{\circ}$  at that distance in  $10^5$  yr.

The offset of TeV J2032+4130 from the center of Cyg OB2 is most easily explained by the existence and location of PSR J2032+4127, i.e., that PSR J2032+4127 is the source of TeV J2032+4130, and not, e.g., winds from O stars in the cluster. In the latter case, it would be difficult to understand why the TeV emission is not more widely distributed among the dozens of O stars of Cyg OB2, and centered on the cluster, which is quite spherical in 2MASS (Knödseder 2000). This argument for associating PSR J2032+4127 with TeV J2032+4130 applies whether or not PSR J2032+4127 is actually in the cluster.

In order to compare the efficiency of TeV gamma-ray production with those of other pulsars listed by Gallant et al. (2008), we integrate the HEGRA spectrum over 0.3–30 TeV, giving  $F(0.3\text{--}30 \text{ TeV}) = 5.1 \times 10^{-12} \text{ erg cm}^{-2} \text{ s}^{-1}$ ,  $L_{\gamma} = 1.8 \times 10^{33} d_{1.7}^2 \text{ erg s}^{-1}$ , and  $\epsilon \equiv L_{\gamma}/\dot{E} = 0.007 d_{1.7}^2$ . This is consistent with the range of efficiencies  $\epsilon = 10^{-4}$ –0.11 found for other PWNe and candidates by Gallant et al. (2008; see also Hessels et al. 2008). Even at  $d = 3.6$  kpc,  $\epsilon = 0.03$  is not exceptional. Also typical for a PWN is the flux of the diffuse X-rays within  $1'$  of PSR J2032+4127,  $\sim 1 \times 10^{-13} \text{ erg cm}^{-2} \text{ s}^{-1}$  in the 0.5–10 keV band (see Figure 8; Mukherjee et al. 2007),

<sup>25</sup> <http://www.mppmu.mpg.de/~rwagner/sources>

which corresponds to  $L_X/\dot{E} \sim 1 \times 10^{-4} d_{1.7}^2$ . Therefore, we approximate the ratio  $L_\gamma/L_X \sim 50$ , which is comparable to the ratio for other older pulsars (Mattana et al. 2009). However, we do not see any evidence for a larger X-ray nebula covering almost the entire HEGRA source that was claimed by Horns et al. (2007) using *XMM* images, with an order of magnitude higher flux than our small nebula.

The spin-down luminosity of PSR J2032+4127 stands out as the smallest of any pulsar identified with a TeV source; the others have  $\dot{E} > 10^{36}$  erg s<sup>-1</sup>. One possible exception is PSR J1702–4128 with  $\dot{E} = 3.4 \times 10^{35}$  erg s<sup>-1</sup>, if it is associated with HESS J1702–420. The latter identification is problematic, however (Aharonian et al. 2008), because it would require  $\epsilon \sim 0.7$  at the estimated distance of 5 kpc, and a rather extreme asymmetry for the TeV emission, peaking more than 0.6 from the pulsar. Nevertheless, the existence of still unidentified TeV sources allows the possibility that new pulsar identifications may be found that are less energetic than the already known pulsar counterparts, and TeV J2032+4130 is probably one such example.

Shortly after the discovery of TeV J2032+4130, Bednarek (2003) proposed that 3EG J2033+4118 is a Vela-type pulsar in Cyg OB2, and that TeV J2032+4130 is its PWN. Using a time-dependent model for the PWN that includes both hadronic and leptonic processes, he assumed a birth period of 2 ms,  $B \sim 6 \times 10^{12}$  G, and present pulsar parameters  $P = 210$  ms and  $\tau_c = 2 \times 10^4$  yr, corresponding to  $\dot{E} = 2.3 \times 10^{35}$  erg s<sup>-1</sup>. The latter is close to the measured value for PSR J2032+4127 of  $\dot{E} = 2.7 \times 10^{35}$  erg s<sup>-1</sup>, although the measured characteristic age of  $1.1 \times 10^5$  yr suggests that the time dependence of the model is not well constrained. For example, PSR J2032+4127 may be too old for its initial spin energy to have had much influence on its present TeV luminosity. See de Jager & Djannati-Ataï (2008) for a discussion of relevant timescales.

Butt et al. (2008) pointed to a possible shell-like arrangement of predominantly non-thermal radio emission, centered on the TeV source, in Very Large Array (VLA) images (see also Paredes et al. 2007). While it is not even clear that this is a single coherent structure, it is unlikely to be the remnant of the supernova that gave birth to the  $\sim 10^5$  yr-old PSR J2032+4127, as its radius of 3 pc at the distance of Cyg OB2 would be too small. Using higher-resolution VLA data, Martí et al. (2007) do not confirm a supernova remnant nature for this emission.

Although PSR J2032+4127 is consistent in position with the Be star MT91 213, there is no other evidence that they are a binary pair such as the prototype gamma-ray emitting binary PSR B1259–63, which has an orbital period of 3.4 yr. Nevertheless, if the proximity of PSR J2032+4127 to Cyg OB2 is real rather than apparent, it is likely that the local radiation background from the massive star cluster enhances inverse Compton TeV emission from the PWN, which might otherwise not have been detectable. Although the total luminosity from massive stars in Cyg OB2 is uncertain, estimates of  $\sim 100$  O stars lead to a luminosity of  $\sim 10^{41}$  erg s<sup>-1</sup>, and a photon energy density of  $\sim 10^2$  eV cm<sup>-3</sup>, which at the location of PSR J2032+4127 may manifest itself mainly as reprocessed IR emission from dust (compared with 0.26 eV cm<sup>-3</sup> for the cosmic microwave background). Detailed modeling, including inverse Compton scattering in the Klein–Nishina regime, will be needed to evaluate the possible TeV emission using this enhanced background radiation, and could help constrain the distance between PSR J2032+4127 and Cyg OB2.

#### 4. CONCLUSIONS

We report radio pulsar detections of two *Fermi* sources previously known only as gamma-ray pulsars, as well as details of their gamma-ray spectra, and probable identifications of their X-ray counterparts. Gamma-ray efficiencies are estimated using their radio dispersion-measure distances. Both pulsars have hard power-law gamma-ray spectra with exponential cutoffs in the GeV band, and large efficiencies relative to spin-down power of  $\sim 0.2$ , assuming isotropic emission. The phase offsets between their radio and gamma-ray pulses follow trends observed in other pulsars, probably indicating their viewing geometry, and consistent with outer magnetosphere models, although more physics must be added to existing calculations to model the detailed structure and spectral evolution of the observed light curves.

PSR J1741–2054 has a low  $\dot{E} = 9.4 \times 10^{33}$  erg s<sup>-1</sup>, and its characteristic age of 0.4 Myr is compatible with the soft X-ray spectral characteristics of its putative counterpart, inferred to be surface thermal emission plus a non-thermal component. With a radio luminosity smaller than that of any other known radio pulsar, PSR J1741–2054 at a distance of 0.4 kpc is approximately twice as far as the radio-quiet, middle-aged gamma-ray pulsar Geminga, which it resembles in its spin-down parameters and X-ray properties. PSR J1741–2054 begins to answer the question of where are the other Gemingas.

PSR J2032+4127 is a more energetic pulsar, with  $\dot{E} = 2.7 \times 10^{35}$  erg s<sup>-1</sup>, and is brighter in radio. A precise timing position derived from a joint fit to *Fermi* and GBT data confines the pulsar position to a region of diffuse X-ray emission previously identified in a *Chandra* image, which is now presumed to be its PWN. The location of PSR J2032+4127 within the extent of the diffuse HEGRA source TeV J2032+4130 solves the 10-year-old mystery of the nature of this, the first unidentified TeV source. PSR J2032+4127 is probably one of the least energetic pulsars powering TeV PWNe, which are now known to be the most numerous type of Galactic TeV source. The location of PSR J2032+4127 projected close to the core of the massive, young stellar association Cyg OB2 at a distance of 1.5–1.7 kpc suggests that this is its true distance, rather than 3.6 kpc estimated from the radio pulsar dispersion.

We thank profusely all the *Fermi* team members who have built and who operate the magnificent spacecraft and LAT experiment. The GBT is operated by the National Radio Astronomy Observatory, a facility of the National Science Foundation operated under cooperative agreement by Associated Universities, Inc. The Parkes Observatory is part of the Australia Telescope, which is funded by the Commonwealth of Australia for operation as a National Facility managed by CSIRO. We are grateful to the *Swift* project scientist and staff for the observation of the LAT PSR J1741–2054 field, and to John Thorstensen for taking the MDM optical spectrum.

The *Fermi* LAT Collaboration acknowledges generous ongoing support from a number of agencies and institutes that have supported both the development and the operation of the LAT as well as scientific data analysis. These include the National Aeronautics and Space Administration and the Department of Energy in the United States, the Commissariat à l’Energie Atomique and the Centre National de la Recherche Scientifique/Institut National de Physique Nucléaire et de Physique des Particules in France, the Agenzia Spaziale Italiana and the Istituto Nazionale di Fisica Nucleare in Italy, the Ministry of Education, Culture,

Sports, Science and Technology (MEXT), High Energy Accelerator Research Organization (KEK) and Japan Aerospace Exploration Agency (JAXA) in Japan, and the K. A. Wallenberg Foundation, the Swedish Research Council and the Swedish National Space Board in Sweden.

*Facilities:* CXO (ACIS-I), Fermi (LAT), GBT (BCPM), GUPPI, Hiltner (RETROCAM), Parkes (PMDAQ), Swift (XRT)

## REFERENCES

- Abdo, A. A., et al. 2007, *ApJ*, **658**, L33
- Abdo, A. A., et al. 2009a, *ApJ*, **700**, 1059
- Abdo, A. A., et al. 2009b, *ApJ*, **699**, L102
- Abdo, A. A., et al. 2009c, *ApJS*, **183**, 46
- Abdo, A. A., et al. 2009d, *ApJ*, **696**, 1084
- Abdo, A. A., et al. 2009e, *ApJ*, **700**, L127
- Abdo, A. A., et al. 2009f, *Science*, **325**, 840
- Abdo, A. A., et al. 2009g, *Science*, **325**, 849
- Aharonian, F., et al. 2002, *A&A*, **393**, L37
- Aharonian, F., et al. 2005, *A&A*, **431**, 197
- Aharonian, F., et al. 2008, *A&A*, **477**, 353
- Albert, J., et al. 2008, *ApJ*, **675**, L25
- Arons, J. 1996, *A&AS*, **120**, 49
- Atwood, W. B., et al. 2009, *ApJ*, **697**, 1071
- Backer, D. C., Dexter, M. R., Zepka, A. D. N., Wertheimer, D. J., Ray, P. S., & Foster, R. S. 1997, *PASP*, **109**, 61
- Becker, W., et al. 2004, *ApJ*, **615**, 897
- Bednarek, W. 2003, *MNRAS*, **345**, 847
- Berghöfer, T. W., Schmitt, J. H. M. M., Danner, R., & Cassinelli, J. P. 1997, *A&A*, **322**, 167
- Butt, Y. M., Combi, J. A., Drake, J., Finley, J. P., Konopelko, A., Lister, M., Rodriguez, J., & Shepherd, D. 2008, *MNRAS*, **385**, 1764
- Butt, Y. M., Drake, J., Benaglia, P., Combi, J. A., Dame, T., Miniati, F., & Romero, G. E. 2006, *ApJ*, **643**, 238
- Camilo, F., Ng, C.-Y., Gaensler, B. M., Ransom, S. M., Chatterjee, S., Reynolds, J., & Sarkissian, J. 2009, *ApJ*, **703**, L55
- Camilo, F., Ransom, S. M., Gaensler, B. M., Slane, P. O., Lorimer, D. R., Reynolds, J., Manchester, R. N., & Murray, S. S. 2006, *ApJ*, **637**, 456
- Camilo, F., et al. 2002, *ApJ*, **571**, L41
- Cohen, D. H., Cassinelli, J. P., & MacFarlane, J. J. 1997, *ApJ*, **487**, 867
- Cordes, J. M., & Lazio, T. J. W. 2002, arXiv:astro-ph/0207156
- de Jager, O. C., & Djannati-Ataï, A. 2008, in *Neutron Stars and Pulsars: 40 Years After Their Discovery*, ed. W. Becker (Berlin: Springer), 451
- Deller, A. T., Tingay, S. J., Bailes, M., & Reynolds, J. E. 2009, *ApJ*, **701**, 1243
- Drew, J. E., Greimel, R., Irwin, M. J., & Sale, S. E. 2008, *MNRAS*, **386**, 1761
- Dyks, J., & Rudak, B. 2003, *ApJ*, **598**, 1201
- Gallant, Y. A., et al. 2008, in *AIP Conf. Ser. 983, 40 Years of Pulsars: Millisecond Pulsars, Magnetars and More*, ed. C. Bassa, Z. Wang, A. Cumming, & V. M. Kaspi (Berlin: Springer), 195
- Halpern, J. P., Camilo, F., & Gotthelf, E. V. 2007, *ApJ*, **668**, 1154
- Halpern, J. P., Gotthelf, E. V., Camilo, F., Helfand, D. J., & Ransom, S. M. 2004, *ApJ*, **612**, 398
- Halpern, J. P., et al. 2008, *ApJ*, **688**, L33
- Han, J. L., Manchester, R. N., Lyne, A. G., Qiao, G. J., & van Straten, W. 2006, *ApJ*, **642**, 868
- Hanson, M. M. 2003, *ApJ*, **597**, 957
- Harding, A. K., Grenier, I. A., & Gonthier, P. L. 2007, *Ap&SS*, **309**, 221
- Hartman, R. C., et al. 1999, *ApJS*, **123**, 79
- Hessels, J. W. T., et al. 2008, *ApJ*, **682**, L41
- Horns, D., Hoffmann, A. I. D., Santangelo, A., Aharonian, F. A., & Rowell, G. P. 2007, *A&A*, **469**, L17
- Hotan, A. W., van Straten, W., & Manchester, R. N. 2004, *PASA*, **21**, 302
- Johnston, S., & Weisberg, J. M. 2006, *MNRAS*, **368**, 1856
- Kassim, N. E., & Lazio, T. J. W. 1999, *ApJ*, **527**, L101
- Kiminki, D. C., et al. 2007, *ApJ*, **664**, 1102
- Knödseder, J. 2000, *A&A*, **360**, 539
- Konopelko, A., et al. 2007, *ApJ*, **658**, 1062
- Lorimer, D. R., & Kramer, M. 2005, *Handbook of Pulsar Astronomy* (Cambridge Univ. Press)
- Manchester, R. N., Hobbs, G. B., Teoh, A., & Hobbs, M. 2005, *AJ*, **129**, 1993
- Manchester, R. N., et al. 2001, *MNRAS*, **328**, 17
- Martí, J., Paredes, J. M., Ishwara Chandra, C. H., & Bosch-Ramon, V. 2007, *A&A*, **472**, 557
- Massey, P., & Thompson, A. B. 1991, *AJ*, **101**, 1408 (MT91)
- Mattana, F., et al. 2009, *ApJ*, **694**, 12
- Morgan, C. W., Byard, P. L., DePoy, D. L., Derwent, M., Kochanek, C. S., Marshall, J. L., O'Brien, T. P., & Pogge, R. W. 2005, *AJ*, **129**, 2504
- Mukherjee, R., Gotthelf, E. V., & Halpern, J. P. 2007, *Ap&SS*, **309**, 29
- Mukherjee, R., Halpern, J. P., Gotthelf, E. V., Eracleous, M., & Mirabal, N. 2003, *ApJ*, **589**, 487
- Neguereuela, I., Marco, A., Herrero, A., & Clark, J. S. 2008, *A&A*, **487**, 575
- Paredes, J. M., Martí, J., Ishwara Chandra, C. H., & Bosch-Ramon, V. 2007, *ApJ*, **654**, L135
- Pellizzoni, A., et al. 2009, *ApJ*, **691**, 1618
- Predehl, P., & Schmitt, J. H. M. M. 1995, *A&A*, **293**, 889
- Radhakrishnan, V., & Cooke, D. J. 1969, *Astrophys. Lett.*, **3**, 225
- Ransom, S. M. 2001, PhD thesis, Harvard Univ.
- Ransom, S. M., Eikenberry, S. S., & Middleditch, J. 2002, *AJ*, **124**, 1788
- Roberts, M. S. E., Hessels, J. W. T., Ransom, S. M., Kaspi, V. M., Freire, P. C. C., Crawford, F., & Lorimer, D. R. 2002, *ApJ*, **577**, L19
- Romani, R. W., & Yadigaroglu, I.-A. 1995, *ApJ*, **438**, 314
- Tauris, T. M., et al. 1994, *ApJ*, **428**, L53
- Thompson, D. J. 2001, in *AIP Conf. Ser. 558, High Energy Gamma-Ray Astronomy*, ed. F. A. Aharonian & H. J. Völk (Berlin: Springer), 103
- Thompson, D. J. 2004, in *Cosmic Gamma-Ray Sources*, ed. K. S. Cheng & G. E. Romero (Dordrecht: Kluwer), 149
- Thompson, D. J., et al. 1999, *ApJ*, **516**, 297
- Watters, K. P., Romani, R. W., Weltevrede, P., & Johnston, S. 2009, *ApJ*, **695**, 1289
- Weltevrede, P., & Johnston, S. 2008, *MNRAS*, **391**, 1210
- Young, M. D., Manchester, R. N., & Johnston, S. 1999, *Nature*, **400**, 848